Hindawi
Wireless Communications and Mobile Computing
Volume 2018, Article ID 6931083, 9 pages
https://doi.org/10.1155/2018/6931083

WILEY | Hindawi

Research Article

LoRa Performance under Variable Interference and Heavy-Multipath Conditions

Kamil Staniec and Michał Kowal

Faculty of Electronics, Telecommunications and Teleinformatics Department, Wroclaw University of Science and Technology, Wroclaw, Poland

Correspondence should be addressed to Kamil Staniec; kamil.staniec@pwr.edu.pl

Received 20 January 2018; Accepted 14 March 2018; Published 24 April 2018

Academic Editor: Kostas Peppas

LoRa (or LoRaWAN) is by far the best known representative of narrowband communication systems designed for the Internet of Things. As a system dedicated specifically for long-range operations, it possesses a considerable processing gain for the energetic link budget improvement and a remarkable immunity to multipath and interference. The paper describes outcomes of measurement campaigns during which the LoRa performance was tested against these two factors, that is, a heavy-multipath propagation and a controlled, variable interference generated, respectively, in a reverberation chamber and an anechoic chamber. Results allow quantitative appraisal of the system behavior under these harsh conditions with respect to LoRa's three major configurable parameters: the spreading factor, bandwidth, and code rate. They also allow dividing LoRa configurational space into three distinct sensitivity regions: in the white region it is immune to both interference and multipath propagation, in the light-grey region it is only immune to the multipath phenomenon but sensitive to interference, and in the dark grey region LoRa is vulnerable to both phenomena.

1. Introduction to LoRa

"LoRaWAN," being an abbreviation of Long-Range WAN [1], is an open communication system dedicated to operation at long distances under harsh attenuation and interference conditions, supported presently by LoRa Alliance. The name "LoRa," in turn, should be understood as a closed, proprietary solution for the LoRaWAN physical layer [2, 3] devised by a French company Cycleo (later purchased by Semtech), based on a variant of the spread spectrum technique, namely, the multistate chirp spread spectrum (CSS). The "multistate" feature means that, as opposed to a generic binary CSS, where each chirp modulates either logical zero or one (by generating, e.g., downchirp and upchirp, resp.), LoRa chirps can modulate from 7 to 12 bits per symbol. It is assumed that LoRa devices are battery-powered offering

(i) high longevity: even up to 10 years under favorable environmental conditions,

(ii) low throughput: up to 21 kb/s with the fastest "LoRa modulation," that is, for SF = 7 and BW = 500 kHz or up to 50 kb/s using FSK modulation,

(iii) long operational distances: 2–5 km in urban and up to 15 km in open or suburban areas.

It is due to these features that LoRa is recognized as one of the most prominent Internet of Things (IoT) systems, which justifies the traction it has gained worldwide. The system can operate in ISM frequency bands at country-dependent operational parameters, such as the radiated power (EIRP), duty cycle (DC), number of channels and their allowed bandwidths (BW), and regulations regarding the use (or not) of "polite spectrum access" mechanisms such as LBT *(Listen Before Talk)* [4] and AFA *(Adaptive Frequency Agility)* [5] or the preamble length. The "regional" specification for LoRa [6] therefore specifies values or states of these parameters in the following frequency ISM bands: EU 433 MHz, CN 470–510 MHz, China 779–787 MHz, US 902–928 MHz, Australia 915–928 MHz, AS 923 MHz, and South Korea 920–923 MHz. The most popular band, however, is by far the EU 863–870 MHz ISM band, especially its "M" and "P" subbands defined in [7], with the following limits on ERP (Equivalent Radiated Power) and DC (duty cycle):

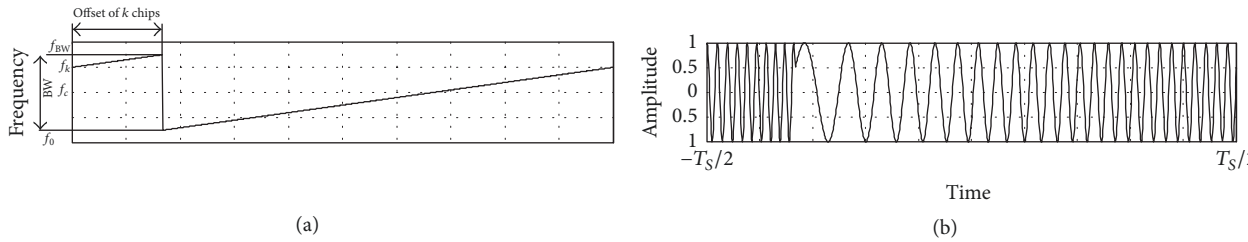

Figure 1: The LoRa modulation: (a) a frequency offset by k chips; (b) a modulated chirp.

(i) "M" subband: 868–868.60 MHz, ERP = 25 mW, and DC ≤ 1%.

(ii) "P" subband: 869.40–869.65 MHz, ERP = 500 mW, and DC ≤ 10%.

In order for up to SF = 12 bits to be encoded in a single LoRa chirp it was necessary to define a unique trajectory within the chirp interval for each of the 2^{SF} symbols (states). It was achieved by assigning each state with an individual offset of k chips on the channel frequency scale (i.e., f_0–f_{BW}), with encoding its value (i.e., the value of a state). In other words, a kth modulation state is encoded by starting a chirp at a frequency f_k being the initial channel frequency f_0 shifted by an offset of k multiples of a chip Δf as in (1) or in Figure 1(a), which depicts a chirp representing a kth modulation state. Thus, each encoded chirp is in fact a cyclically shifted (by k chips) version of the reference signal (that starts from f_0), which results in an abrupt frequency change in the kth chip (sample) of the modulated chirp, as shown in Figure 1(b) for $k = 167$. Owing to this principle, the method allows obtaining a multistate chirp modulation (within the range of 2^7–2^{12} of individual states), as opposed to the classical binary chirp modulation.

$$f_k = f_0 + k \cdot \Delta f = f_0 + k \cdot \frac{\mathrm{BW}}{2^{\mathrm{SF}}}. \tag{1}$$

The instantaneous frequency f_i is given by (2), where f_c is the chirp carrier frequency, centered about −BW/2 and +BW/2. Moreover, in order to provide the highest possible Hamming distance, k chips are also Gray coded for improving error detection/correction receiver capabilities. The Forward Error Correction is provided by the selection of one of four coding efficiencies $R = \{0.5; 0.57; 0.67; 0.8\}$ defined by formula (3), depending on the, so-called, coding rate (CR) that can be 1, 2, 3, or 4.

$$f_i(t) = \begin{cases} f_c + \dfrac{\mathrm{BW}}{T_s}\left(t - \dfrac{k}{T_s}\right) + \mathrm{BW} & \text{dla } -\dfrac{T_s}{2} \le t < \dfrac{k}{\mathrm{BW}} \\ f_c + \dfrac{\mathrm{BW}}{T_s}\left(t - \dfrac{k}{T_s}\right) & \text{dla } \dfrac{k}{\mathrm{BW}} \le t \le \dfrac{T_s}{2}. \end{cases} \tag{2}$$

$$R = \frac{4}{4 + \mathrm{CR}}. \tag{3}$$

The chirp signal spectral width BW can vary between 125 kHz, 250 kHz, and 500 kHz (shown in Figure 2), which along with the spreading factor SF, the chirp signal duration T_s, and the coding efficiency R, lends itself to calculating the bit rate R_b as in (4). Calculation performed for various combinations of BW and SF with extreme values of R (i.e., 0.5 and 0.8) have been provided in Table 1. From (4) for the symbol duration T_s one can arrive at an expression for the chip rate R_c given by formula (5), which brings a conclusion that the spread data stream in LoRa is sent at a chip rate equal to the channel bandwidth BW.

$$R_b = \mathrm{SF} \cdot T_s \cdot R = \mathrm{SF} \cdot \left\lceil \frac{\mathrm{BW}}{2^{\mathrm{SF}}} \right\rceil \cdot \frac{4}{4 + \mathrm{CR}} \ \ [\mathrm{b/s}] \tag{4}$$

$$T_s = \frac{2^{\mathrm{SF}}}{\mathrm{BW}} \ \ [\mathrm{s}] \Longrightarrow \quad R_s = \frac{1}{T_s} = \frac{\mathrm{BW}}{2^{\mathrm{SF}}} \ \ [\mathrm{symbols/s}] \tag{5}$$

$$R_c = R_s \cdot 2^{\mathrm{SF}} \ \ [\mathrm{c/s}] \Longrightarrow \quad R_c = \frac{\mathrm{BW}}{2^{\mathrm{SF}}} \cdot 2^{\mathrm{SF}} = \mathrm{BW} \ \ [\mathrm{c/s}]. \tag{6}$$

This means that in every second there are just as many chips sent as the number of Hz that have been swept in the meantime. On top of that it should be mentioned that chirps spread out with different SFs are orthogonal with respect to each other and thus can be considered as separate "logical" channels, each identified by its own SF value, that can further be bundled into aggregate channels with a combined capacity being a sum of bit rates of its constituent logical channels, as also shown in the bottom row of Table 1. The choice of SF, R, and BW, however, should also be affected by the quality of propagation conditions, with higher values of SF and R while having lower BW in harsher conditions (i.e., high attenuation interference) and opposite settings in more benign circumstances (leading also to higher bit rates).

2. Interference-Prone IoT Environment

The IoT system operation in unlicensed ISM bands on one hand entails the lack of license fees; on the other hand, however, the shared use of the spectrum causes inevitable rise of the background noise, as new radiating devices are being added. The issue of this elevated noise was tackled, for instance, in [8], where wideband measurements (for the range 200–3000 MHz) were carried out in urban environments in

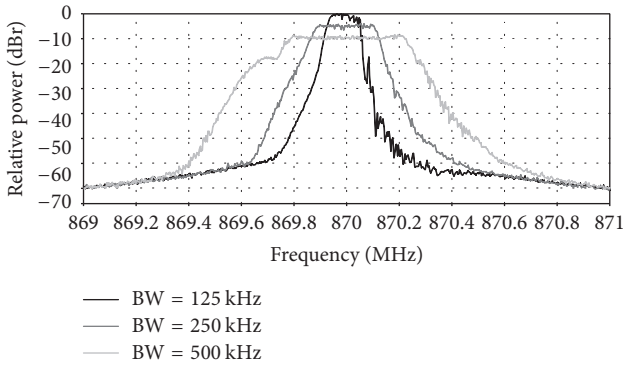

Figure 2: LoRa spectrum measured for different bandwidths.

Table 1: The bit rate R_b and the aggregate capacity C_{b_ch} of LoRa.

BW →	125 kHz		250 kHz		500 kHz	
R →	0.5	0.8	0.5	0.8	0.5	0.8
SF ↓	Bit rate R_b [kb/s]					
7	3.42	5.47	6.84	10.94	13.67	**21.88**
8	1.95	3.13	3.91	6.25	7.81	12.50
9	1.10	1.76	2.20	3.52	4.39	7.03
10	0.61	0.98	1.22	1.95	2.44	3.91
11	0.34	0.54	0.67	1.07	1.34	2.15
12	**0.18**	0.29	0.37	0.59	0.73	1.17
Aggregate capacity C_{b_ch} [kb/s]	**7.6**	**12.17**	**15.21**	**24.32**	**30.38**	**48.64**

2016. It was demonstrated there that in comparison to analogous data gathered in 2004 [9] the average spectral occupancy was increased considerably indicating the appearance of a plethora of new radiation sources (located more densely) that had appeared over that period. They are characterized by a high unpredictability and a considerable variance both in time and in amplitude which do not allow qualifying them as white Gaussian noise. The main contributors of expected radiations, of course, have been identified to be the cellular systems (GSM, UMTS, and LTE) and DVB-T. There are, however, also unexpected events with random characteristics, hardly describable with statistical models, such as passing-by of a vehicle emitting EM waves from its board communications and signals emitted from remote controls for opening doors and gates and from home automation systems. Indoor radiation may come from any computer equipment (especially server rooms), WLANs, or computer peripherals communicating by Bluetooth. This raised background noise inside buildings may turn out particularly harmful to IoT systems, which by definition are dedicated for acquiring data from indoor locations and sending them via modems located directly in/at meters and sensors.

A similar long-term measurement campaign of this ambient noise within the ISM 868.0–868.6 MHz band was carried out in Aalborg (Denmark, 2017) and reported in [10]. It was observed there that 22% of measured samples could be qualified as high, that is, at power levels in excess of −105 dBm, among which many were found to be close to −65 dBm. The best-fit model for this probability density profile was found to be the Generalized Extreme Value (GEV) Distribution (rather than Gaussian), typically used to describe extreme phenomena (and for this reason often used in meteorology and hydrology). Some other interesting research presented there also indicated the anticipated influence of this type of GEV-modeled background noise on the operation of LoRa and SigFox—both deemed as representatives of two major groups of noncellular IoT systems, namely, LPWAN (Long-Range WAN) and UNB (Ultra-Narrow Band), respectively. As was demonstrated, due to this increased background noise the simulated effective range is expected to drop down to 78% (LoRa) or 50% (SigFox) of the reference nominal range achieved under interference-free conditions. This means that even despite the tripled transmission of each packet with SigFox, each on a different randomly selected carrier frequency, it still appears to be more susceptible to interference than LoRa which owes its high immunity to adverse conditions to its considerable processing gain found to be between 11 dB (for SF = 7, $R = 0.8$) and 23 dB (for SF = 12, $R = 0.8$). As for the influence of a single-tone interference, measurements documented in [11] indicate that this type of disturbance has no significant effect as long as it does not exceed LoRa signal power by 5 dB for SF = 7 and 19.5 dB for SF = 12, given the coding efficiency $R = 0.67$ (i.e., for CR = 2). Other valuable contributions to the topic of interference in LoRa are [12–16].

3. Interference Background for LoRa

An issue of possible electromagnetic interference affecting IoT networks was noticed in ETSI TR 102 691 [17] to take place in the access segment between the sensors/meters layer and the Access Points (AP) layer. The document deals with the topic in general terms, by introducing potential targets and consequences that EM interference may have on Machine-To-Machine (M2M) systems, which are target "clients" of IoT, as well as by presenting some recommendable countermeasures. In particular, two main interference sources have been identified: intentional and unintentional. The former are most often intended to gain access to the telemetric data in transit or their modification. The latter, in turn, occur due to adverse EM interactions that may disturb connectivity between IoT end-devices and their respective AP. As for LoRa, one can identify two such sources: LoRa signals and other signals. The first type of threat may occur during simultaneous transmission to/from two more LoRa-enabled devices with the use of exactly the same set of transmission parameters: $\{f_c; \text{BW}; \text{SF}\}$. In that case individual chirp signals would not be mutually orthogonal any more, whereby making it impossible to discriminate between such transmissions in the detector. By careful planning of the AP deployment on a given area the likelihood of such situations should be reduced. Even harder to predict and control are interferences arriving from sources other than LoRa transmitters, yet sharing the same frequency band. The following chapters will be devoted to the investigations of influence that the factors mentioned below have on the Packet Error Rate (PER) in LoRa devices:

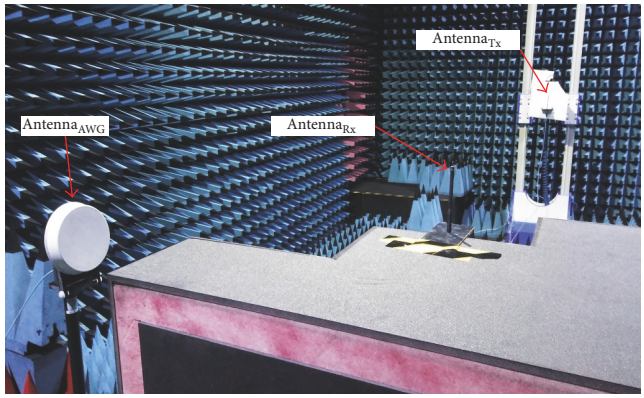

Figure 3: A photo of the measurement set-up inside the anechoic chamber of LKE (WUST).

(i) Electromagnetic interference of a variable power level and a constant time-spectral characteristic (conditions adequate for emulation were obtained in an anechoic chamber (Section 4))

(ii) Extremely multipath propagation, obtained in a reverberation chamber (Section 5).

4. Measurement of LoRa Susceptibility to Interference

In order to better imitate the background noise rise as a major wideband source of interference to LoRa in the investigations, a continuous 1000-kHz wide AWGN signal was generated by a Tektronix AWG 7000 arbitrary signal generator (interferer) with the output power P_{gen} set to 7 dBm. This level was selected so that in the process of switching between different values of SF one could observe transitions between PER = 0% and PER = 100%. P_{gen} was then decreased in 3 dB steps down to the level of −8 dBm, which allowed observing the influence of successively increasing SNR on the resultant Packet Error Rate. The aim of this research was to provide quantitative and objective conclusions regarding the advisable settings of BW, SF, and R in response to the quality of interference-related and multipath-related conditions. The measurement platform was set up in an anechoic chamber of the Laboratory of Electromagnetic Compatibility (LKE) at Wroclaw University of Technology (WUST) and shown in Figure 3. For further reduction of any unexpected spurious radiation other than that taking place between the LoRa devices and the interferer, only three antennas were located inside the chamber, as schematically presented in Figure 4. The signal generator as well as LoRa transmitter and receiver modules were placed outside.

The anechoic chamber itself provided 85 dB of shielding effectiveness from external EM environment, which guaranteed that the only source of interfering field was the intentional AWGN signal. The LoRa devices used in experiments were Eiger platform modules based on Semtech SX1276 chipsets. In each sample measurement a setting consisting of a unique combination of the aforementioned LoRa operational parameters, namely, {BW, SF, R}, was used. Moreover, since the packet total transmit time for LoRa varied with these three parameters, the measurement of each sample lasted until the observed PER was stabilized. The entire measurement matrix therefore consisted of three settings for BW (125 kHz, 250 kHz, and 500 kHz), six for SF (7–12), four for R (0.8, 0.67, 0.57, and 0.5), and six for P_{AWG} (7 dBm, 4 dBm, . . ., −8 dBm), yielding 432 individual measurements, presented in Figure 5.

A closer analysis of the presented results leads to the following three major takeaways regarding the effect of BW, SF, and R on the resultant PER.

Conclusion 1. It stems from analyzing the horizontal distribution of PER profiles within each BW as they shift from left (high index SF, i.e., 12) towards right as SNR is being increased in response to lowering the interfering power P_{gen}. One can easily notice a certain regularity in PER behavior as a function of SNR; namely, low PER regions (i.e., those close to 0%) tend to be shifting by one SF index to the right per every 3-dB (or, in few cases, 2-dB) increase in SNR. For instance, the low PER region moves from SF = 12 to SF = 11 for BW = 500 kHz (as SNR changes from −19 dB to −16 dB) or from SF = 10 to SF = 9 for BW = 125 kHz (as SNR changes from −8 dB to −5 dB).

Conclusion 2. Remembering that SNR can be changed not only by means of lowering the interferer power but also by changing the channel bandwidth BW, another straightforward inference can be deduced from observing the vertical PER profiles in the figure. It appears that each downscaling of BW by a factor of two (i.e., from 500 kHz to 250 kHz or from there to 125 kHz) causes the low PER region to extend by one SF index to the right:

(i) For BW = 500 kHz low PER region contains only SF = {12}.

(ii) For BW = 250 kHz low PER region contains SF = {11, 12}.

(iii) For BW = 125 kHz low PER region contains SF = {10, 11, 12}.

Conclusion 3. As for the coding efficiency R influence, its value was varied four times within each SF region, toggled between 0.5 through 0.8. As could be expected, PER was growing along the growing R, assuming the lowest values at the left edge of each SF region, where the transmission had the strongest protection with $R = 0.5$, and reaching the highest levels near the right edge corresponding to the least error-protected scenario with $R = 0.8$. Due to these four possible values of R the transitions between extreme PER states (i.e., 0% and 100%) do not occur abruptly but rather follow smooth slopes as R varies between 0.5 and 0.8 where the 0–100% PER transitions occur.

5. Measurement of LoRa Susceptibility to Multipath Propagation

As is well known, any emitted signal will propagate by interacting with the surrounding environment, which involves reflections from objects, transmissions through obstacles,

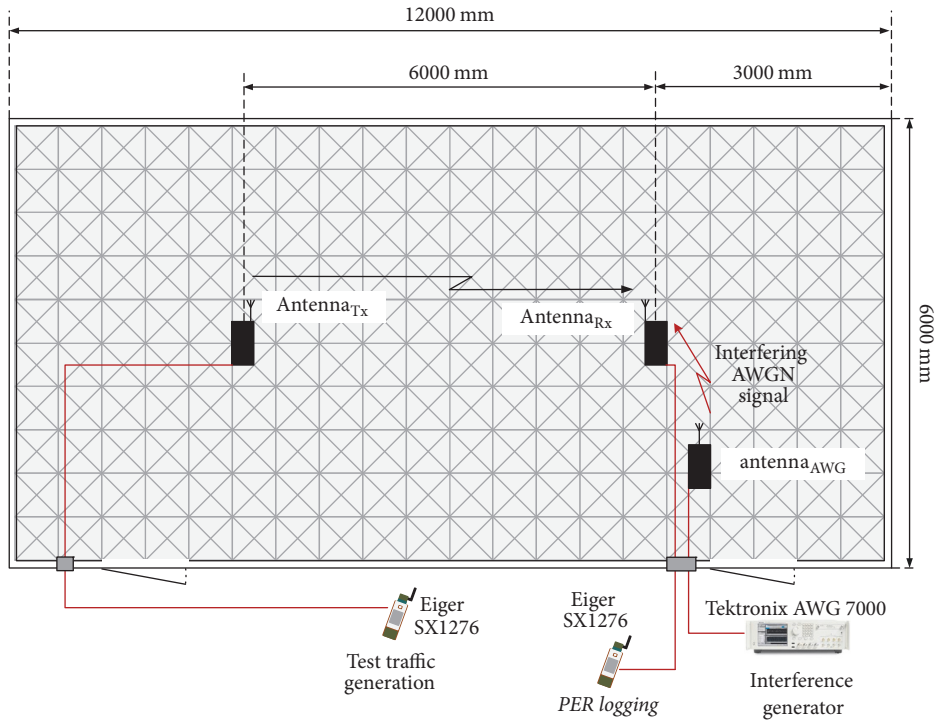

Figure 4: A schematic of the set-up used for measuring LoRa performance in LKE (WUST) anechoic chamber.

diffraction on edges, and scattering from rough surface. Thus, the signal arriving at the receiver will not come in a single fringe but as a bundle of signals with different amplitudes, phases, angles of arrival, and short time delays, being delayed copies of the original signal. Once collected within a certain time interval at a receiver, they sum up in a vector fashion, accounting for their relative phase differences, which causes some copies to overlap constructively if both are in phase or cancel out otherwise. Such behavior leads to small-scale fading, which is a typical propagation effect, especially in the indoor and urban environment. Hence, the radio channel can be mathematically represented at any point in a three-dimensional space as a linear, time-variant filter of an impulse response given by (7) or as a Power Delay Profile (PDP) defined by (8) [18]. In the formula $h(t, \tau)$ is the radio channel impulse response, $N_{\text{multipath}}$ is the number of multipath components, and $\theta_i(t)$ and $E_i(t)$ are, respectively, the time varying phase and electric field amplitude of each echo, while τ_i is its delay. The time variance τ appears here due to the temporal changes in real propagation environments, such as the motion of people and relocation of objects. It should be included to reflect the fact that in usual circumstances, with nonstationary channel, a given PDP will vary over time even when measured at exactly the same location but, for example, at different hours of the day.

$$h(t, \tau) = \sum_{i=0}^{N(\tau)-1} E_i \delta(t - \tau_i, \tau) e^{j\theta_i(t,\tau)}, \tag{7}$$

$$\text{PDP}(t, \tau) = \sum_{i=0}^{N(\tau)-1} P_i \delta(t - \tau_i, \tau), \tag{8}$$

$$\tau_{\text{RMS}} = \sqrt{\frac{\sum_i (\tau_i - \tau_m)^2 \cdot P(\tau_i)}{\sum_i P(\tau_i)}}, \tag{9}$$

$$\tau_m = \frac{\sum_i \tau_i \cdot P(\tau_i)}{\sum_i P(\tau_i)}. \tag{10}$$

A common statistical measure of the channel dispersiveness is the excess time delay spread τ_{RMS}, having a sense of the second central moment of the PDP, as in (9), and determining the maximum symbol rate achievable by a communication system without occurrence of the intersymbol interference (ISI). The harshest propagation environments, in terms of the multipath propagation, are those characterized by the greater values of τ_{RMS} (above 1 μs) such as hilly or mountainous terrains and suburban/urban macrocells, whereas indoor and microcellular spaces usually possess τ_{RMS} on the order of tens (indoor) up to hundreds (microcells) of nanoseconds [19].

Multipath propagation conditions can be easily emulated in a reverberation chamber, such as one schematically presented in Figure 6, wherein τ_{RMS} is controlled by means of adding or subtracting absorbing panels within a wide range of values. In the chamber of interest (LKE, WUST) this range spanned from 1.55 μs in case of an unloaded chamber, that is, void of absorbers, down to 0.2 μs with 12 absorbers on the chamber walls, as demonstrated in [20]. In the experiment carried out in a configuration presented in Figure 6, the chamber was unloaded (thus $\tau_{\text{RMS}} = 1.55$ μs) for testing LoRa performance under extremely multipath conditions, such as those typically encountered in urban/suburban environments which, at the same time, are the target deployment locations for IoT systems. LoRa receiver and transmitter

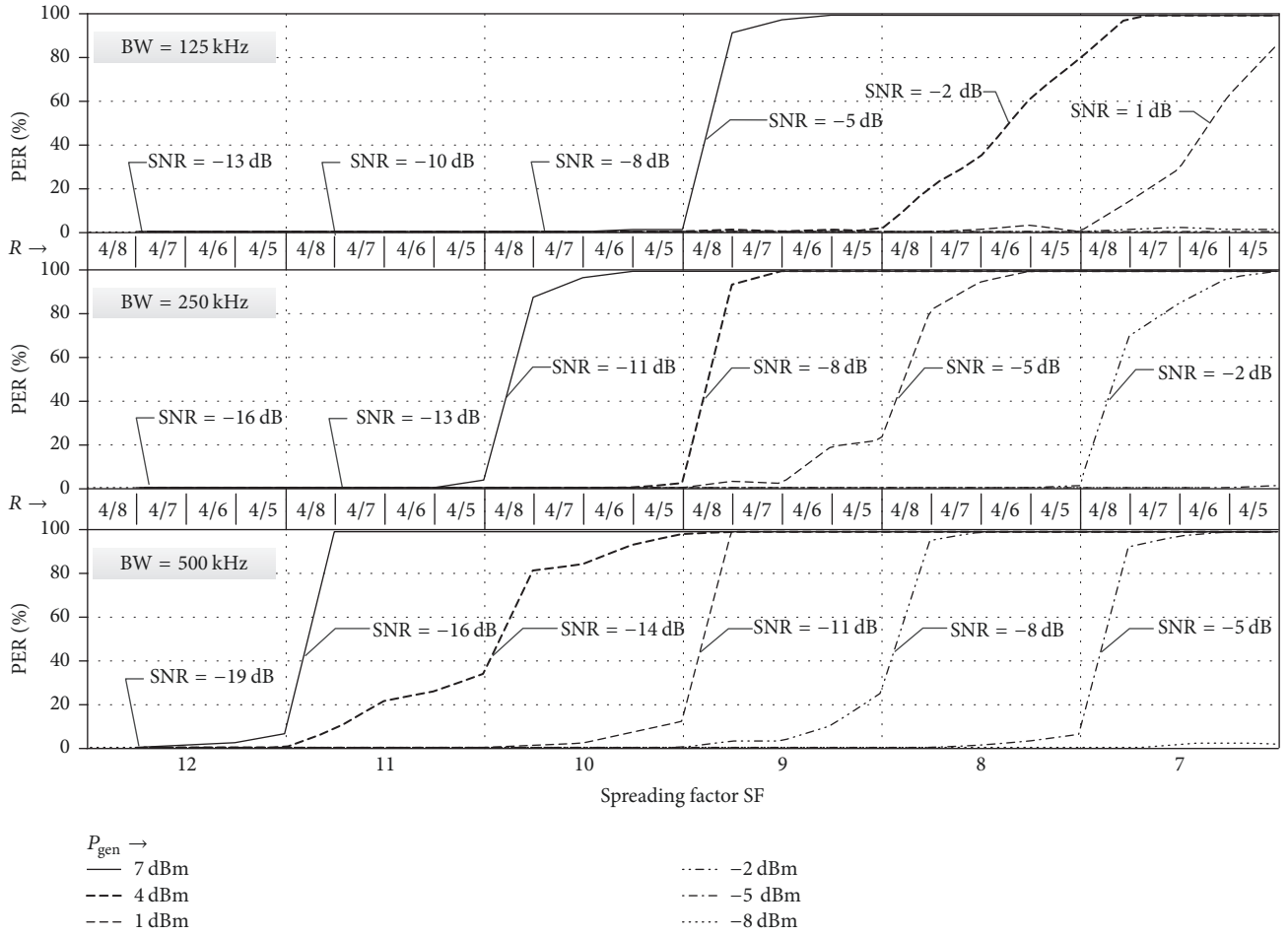

Figure 5: Packet Error Rate measurements for LoRa obtained in the anechoic chamber.

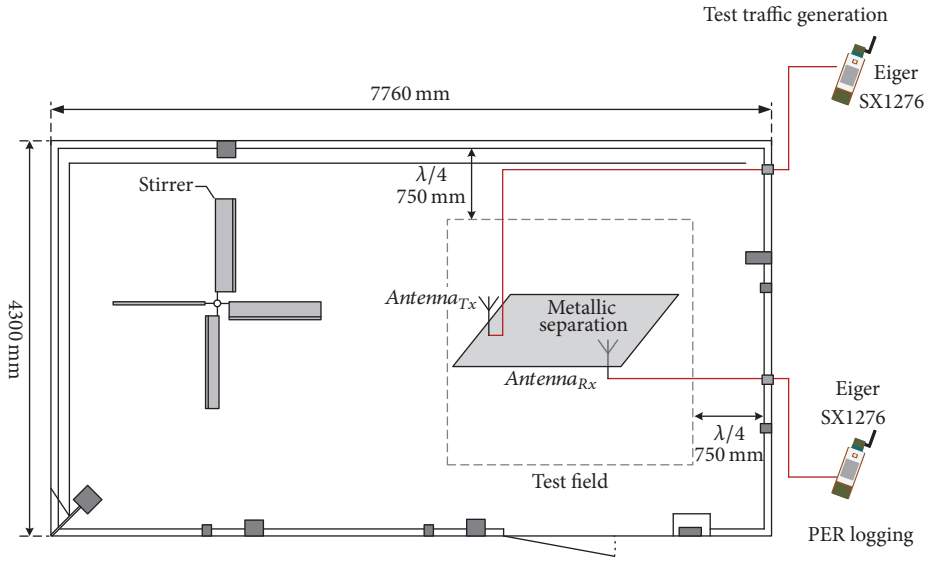

Figure 6: A schematic of the set-up used for measuring LoRa performance in LKE (WUST) reverberation chamber.

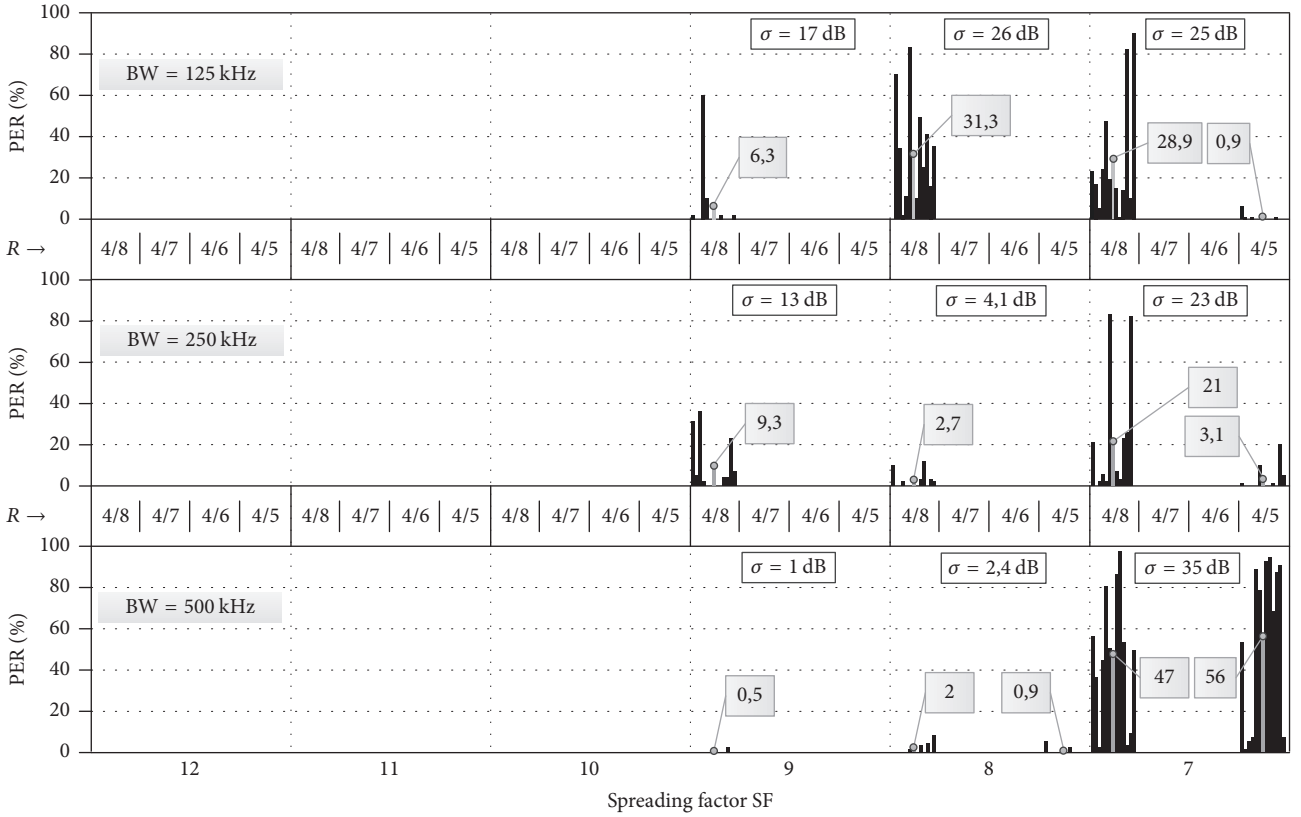

Figure 7: Packet Error Rate measurements for LoRa obtained in the LKE (WUST) reverberation chamber.

antennas were placed in the test field, defined as an area away from the chamber walls by at least $\lambda_{max}/4$, where is λ_{max} is the longest wavelength to be propagated inside the cavity (here, λ_{max} = 3 m which corresponds to the lowest operational frequency f_L equal to 100 MHz).

In the measurements, Tx and Rx antennas were separated by a metallic sheet to prevent line-of-sight (LOS) conditions and obtain the Rayleigh channel (desirable and typical for resonant cavities such as the reverberation chamber [21]), that is, one where the reception is only possible via purely multipath propagation. Similarly to the interference susceptibility measurements described in Section 4, LoRa devices were again tested for three possible BW = {125 kHz; 250 kHz; 500 kHz} and six spreading factors SF = {7–12} but only two extreme coding efficiencies $R = \{0.5; 0.8\}$. Moreover, in order to comply with IEC 61000-4-21 Part, 4-norm [22], the measurement of each triplet combination (BW, SF, R) was carried out twelve times, that is, once per every stirrer position, changed in steps of 30°, thus eventually covering the full stirrer rotation. According to [22] such a number of positions guarantee measurement uncertainty at a 95% confidence level and are applicable to the frequency range $6 \cdot f_L$–$10 \cdot f_L$ which in case of the WUST LKE reverberation chamber is equivalent to 600–1000 MHz, a range containing the center frequency used in the tests (f_c = 870 MHz).

Analysis of results presented in Figure 7 leads to the following conclusions.

Conclusion 1. Similarly to the investigations on EM interference, greater SF leads to an increased immunity to the strongly multipath propagation in the Rayleigh channel. It is evident that for the three highest SF indices (12–10) LoRa is virtually insensitive to the multipath and yields PER = 0%, irrespective of the channel bandwidth BW. Beginning with SF = 9, in turn, at certain stirrer positions there appear high peaks in PER, reaching 60% for BW = 125 kHz, ending with SF = 7 where, at the same bandwidth, PER readings exceeding 80% were reported.

Conclusion 2. The influence of BW on the sensitivity to the multipath propagation does not seem to be as obvious as that for SF in the previous conclusion. Accepting PER averaged over all 12 stirrer positions as a reliable indicator, smaller values of BW appear to be more sensitive producing at BW = 125 kHz PER of 6.4% and 31.3% for SF = 9 and 8, respectively. However, for BW = 500 kHz channels, PER for the same two SFs is rather negligible (between 0.5% and 2.0%). But, then, outcomes obtained for SF = 7 (and still BW = 500 kHz) again conform with the assumption that the lowest immunity is attained for the widest channels, since PER in that region equal to 47% and 56%, respectively, for R equal to 0.5 and 0.8, is far in excess of values in the other two channel bandwidths.

Conclusion 3. The measured LoRa responses to the multipath channel, in terms of PER, exhibit remarkable variability over 12 stirrer positions. Its quantitative evaluation was therefore

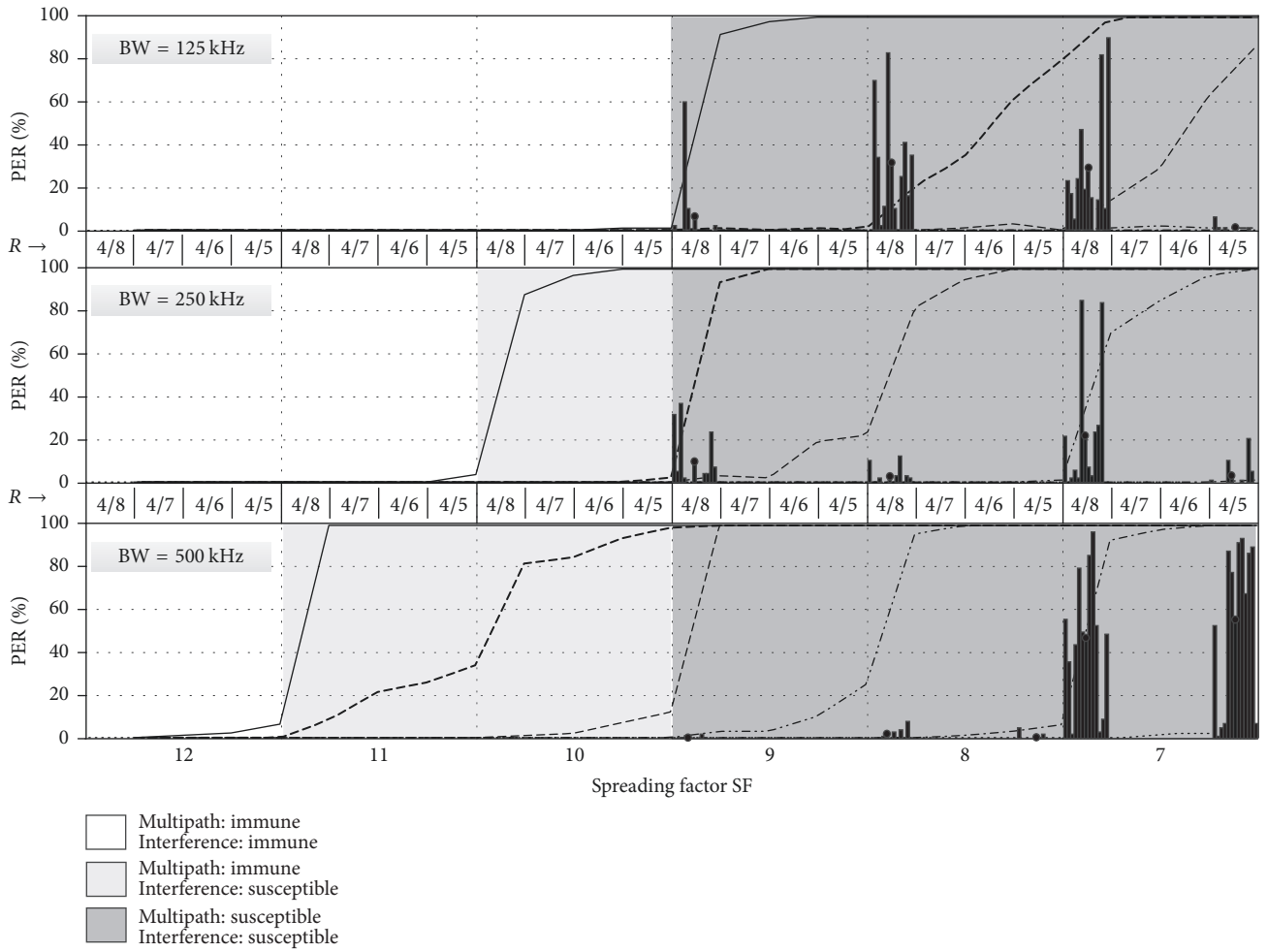

Figure 8: A combined set of results of PER measurements for LoRa obtained for the EM interference (anechoic chamber) and the multipath propagation (reverberation chamber).

only possible by introducing the standard deviation σ calculated for each separate set of 12 PERs shown in the figure. Very high values of σ, reaching 35 dB, seem to indicate that average PER discussed in Conclusion 2 is burdened with too great uncertainty to be treated as reliable indicator of the multipath influence.

Considering the above three conclusions, one should agree that perhaps the most credible statement regarding the influence of the multipath propagation on the LoRa performance is one included in Conclusion 1. It states that out of the three configurable parameters (SF, BW, and R), only SF has an apparent influence on PER, by providing a clear division of the configurational space into two regions: the multipath-immune (or 0% PER) region for SF = 12–10 and the multipath-sensitive (100% PER) region for SF = 9–7.

6. Conclusions

The outcomes presented in the paper provide a quantitative confirmation of the general rules regarding recommendable settings for LoRa, in terms of SF, BW, and R. This rule states that, under conditions of high EM interference, it is advisable to use smaller channel bandwidths BW and higher spreading factors SF.

In Section 4 a straightforward dependency was demonstrated between BW and SF indicating that each twofold reduction of BW extends the pool of safe operational regions (i.e., those interference-immune with PER ≈ 0%) by one SF index. For example, for BW = 500 kHz the safe region only contained SF11, whereas the narrowing of BW down to 250 kHz appends to this region also SF11.

As for the immunity to the multipath propagation, results presented in Section 5 reveal that irrespective of the channel bandwidth BW, LoRa exhibits no susceptibility for SF = 12–10, whereas for the other spreading factors (i.e., 9–7) a remarkable sensitivity can be observed, although greatly varied and hard to express in quantitative terms.

In Figure 8 results from both parts of investigations were combined, namely, the EM interference and the multipath interference, leading to further practical conclusions of possibly real importance to the design process of an IoT network based on the LoRa system. Namely, out of all operational regions (defined by individual indices of SF) three major

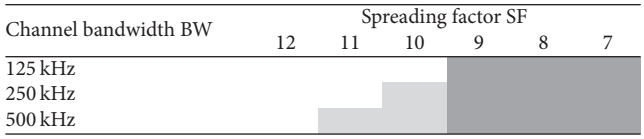

Figure 9: A schematic division of the LoRa configurational space into distinct regions of immunity and susceptibility for the EM interference and the multipath propagation.

groups can be distinguished with respect to LoRa's immunity to the EM interference and the multipath propagation. They were marked with white, bright grey, and dark grey colors (also shown, for clarity, in Figure 9):

(i) The white region, in which LoRa is characterized by immunity to both the EM interference and the multipath propagation

(ii) The bright grey region, in which LoRa preserves immunity to the multipath propagation but reveals susceptibility to the EM interference

(iii) The dark grey region, in which LoRa is strongly influenced by both the EM interference and the multipath propagation.

Conflicts of Interest

The authors declare that they have no conflicts of interest.

Acknowledgments

This paper has been written as a result of realization of the Wroclaw University of Science and Technology Internal Grant entitled "Development of Modern Information and Communication Techniques: A Continuation," no. 0401/0140/17.

References

[1] A. Lavric and V. Popa, "Internet of things and LoRa™ low-power wide-area networks: a survey," in *Proceedings of the 2017 International Symposium on Signals, Circuits and Systems, ISSCS 2017*, Iasi, Romania, July 2017.

[2] N. Sornin, M. Luis, T. Eirich, T. Kramp, and O. Hersent, "LoRaWAN Specification," Version: V1.0.2, July 2016.

[3] Semtech, "LoRa modulation basics," Application Note AN1200.22.

[4] ETSI, "Electromagnetic compatibility and Radio spectrum Matters (ERM); Frequency-agile Generic Short Range Devices using Listen-Before-Transmit (LBT)," Tech. Rep. TR 102 313 V1.1.1 (2004-07), 2004.

[5] ETSI, "Short Range Devices (SRD) operating in the frequency range 25 MHz to 1,000 MHz; Part 2: Harmonised Standard covering the essential requirements of article 3.2 of Directive 2014/53/EU for non specific radio equipment," Tech. Rep. EN 300 220-2 V3.1.1 (2016-11), 2016.

[6] LoRa Alliance Technical committee, "LoRaWAN Regional Parameters," Version: V1.0, July 2016.

[7] The European table of frequency allocations and applications in the frequency range 8.3 kHz to 3000 GHz (ECA Table).

[8] A. Palaios, V. Miteva, J. Riihijarvi, and P. Mahonen, "When the whispers become noise: a contemporary look at radio noise levels," in *Proceedings of the 2016 IEEE Wireless Communications and Networking Conference, WCNC 2016*, Doha, Qatar, April 2016.

[9] M.-H. Chang and K.-H. Lin, "A comparative investigation on urban radio noise at several specific measured areas and its applications for communications," *IEEE Transactions on Broadcasting*, vol. 50, no. 3, pp. 233–243, 2004.

[10] B. Vejlgaard, M. Lauridsen, H. Nguyen, I. Z. Kovacs, P. Mogensen, and M. Sørensen, "Interference impact on coverage and capacity for low power wide area IoT networks," in *Proceedings of the 2017 IEEE Wireless Communications and Networking Conference, WCNC 2017*, San Francisco, Calif, USA, March 2017.

[11] SX 1272/3/6/7/8: LoRa Modem, Semtech, Designer's Guide, AN1200.13, rev 1, July 2013.

[12] A. Aloÿs, J. Yi, T. Clausen, and W. M. Townsley, "A Study of LoRa: long range & low power networks for the internet of things," *Sensors*, vol. 16, no. 9, article 1466, 2016.

[13] M. Lauridsen, B. Vejlgaard, I. Z. Kovacs, H. Nguyen, and P. Mogensen, "Interference measurements in the European 868 MHz ISM band with focus on LoRa and SigFox," in *Proceedings of the 2017 IEEE Wireless Communications and Networking Conference, WCNC 2017*, San Francisco, Calif, USA, March 2017.

[14] C. Orfanidis, L. M. Feeney, M. Jacobsson, and P. Gunningberg, "Investigating interference between LoRa and IEEE 802.15.4g networks," in *Proceedings of the 2017 IEEE 13th International Conference on Wireless and Mobile Computing, Networking and Communications (WiMob)*, pp. 1–8, Rome, Italy, October 2017.

[15] J. Haxhibeqiri, F. Van den Abeele, I. Moerman, and J. Hoebeke, "LoRa scalability: a simulation model based on interference measurements," *Sensors*, vol. 17, no. 6, article 1193, 2017.

[16] T. Voigt, M. Bor, U. Roedig, and J. Alonso, "Mitigating Inter-network Interference in LoRa Networks," in *Proceedings of the International Conference on Embedded Wireless Systems and Networks (EWSN)*, pp. 323–328, Uppsala, Sweden, February 2017.

[17] ETSI, "Machine-to-Machine communications (M2M); Smart Metering Use Cases," ETSI TR TR 102 691 V1.1.1 (2010-05), 2010.

[18] ITU, "Multipath propagation and parameterization of its characteristics," Tech. Rep. ITU-R P.1407-1, 1999.

[19] S. R. Saunders and A. Aragón-Zavala, *Antennas and Propagation for Wireless Communications Systems*, John Wiley & Sons, New York, NY, USA, 2nd edition, 2007.

[20] A. J. Pomianek, K. Staniec, and Z. Joskiewicz, "Practical remarks on measurement and simulation methods to emulate the wireless channel in the reverberation chamber," *Progress in Electromagnetics Research*, vol. 105, pp. 49–69, 2010.

[21] D. A. Hill, "Electromagnetic fields in cavities: deterministic and statistical theories," in *The IEEE Press Series on Electromagnetic Wave Theory*, John Wiley & Sons, 2009.

[22] IEC 61000-4-21 Electromagnetic compatibility (EMC) Part 4: Testing and measurement techniques Reverberation chamber test methods. Section 21: Reverberation Chamber Test Methods.